Multimodality Assessment of Brain Tumors and Tumor Recurrence

Wolf-Dieter Heiss[1], Peter Raab*[2], and Heinrich Lanfermann*[2]

[1]Max Planck Insitute for Neurological Research, Cologne, Germany; and [2]Institute for Diagnostic and Interventional Neuroradiology, Hannover Medical School, Hannover, Germany

Learning Objectives: On successful completion of this activity, participants should be able to describe (1) the differences in the information obtained by various MRI and PET modalities and (2) the best combination of imaging procedures to detect brain tumors, to define the biologic activity or malignancy of a tumor, to validate therapeutic effects, and to differentiate between recurrent tumor and tissue necrosis.

Financial Disclosure: The authors of this article have indicated no relevant relationships that could be perceived as a real or apparent conflict of interest.

CME Credit: SNM is accredited by the Accreditation Council for Continuing Medical Education (ACCME) to sponsor continuing education for physicians. SNM designates each JNM continuing education article for a maximum of 1.0 AMA PRA Category 1 Credit. Physicians should claim only credit commensurate with the extent of their participation in the activity.

For CE credit, participants can access this activity through the SNM Web site (http://www.snm.org/ce_online) through October 2012.

Neuroimaging plays a significant role in the diagnosis of intracranial tumors, especially brain gliomas, and must consist of an assessment of location and extent of the tumor and of its biologic activity. Therefore, morphologic imaging modalities and functional, metabolic, or molecular imaging modalities should be combined for primary diagnosis and for following the course and evaluating therapeutic effects. MRI is the gold standard for providing detailed morphologic information and can supply some additional insights into metabolism (MR spectroscopy) and perfusion (perfusion-weighted imaging) but still has limitations in identifying tumor grade, invasive growth into neighboring tissue, and treatment-induced changes, as well as recurrences. These insights can be obtained by various PET modalities, including imaging of glucose metabolism, amino acid uptake, nucleoside uptake, and hypoxia. Diagnostic accuracy can benefit from coregistration of PET results and MRI, combining the high-resolution morphologic images with the biologic information. These procedures are optimized by the newly developed combination of PET and MRI modalities, permitting the simultaneous assessment of morphologic, functional, metabolic, and molecular information on the human brain.

Key Words: neurology; oncology; brain tumors; gliomas; PET; MRI

J Nucl Med 2011; 52:1585–1600
DOI: 10.2967/jnumed.110.084210

Brain tumors are newly formed alterations of morphology, and for their diagnosis, therefore, CT or MRI is mandatory. These imaging modalities are essential for delineating the normal and pathologic anatomy and also for assessing vascular supply and impairment of the blood–brain barrier (BBB) (perfusion-weighted imaging; contrast enhancement). Additionally, MRI is capable of giving functional information on microstructural (diffusion-weighted imaging [DWI]), physiologic, and metabolic (MR spectroscopy [MRS]) changes of tumor tissues. PET and MRI provide physiologic, biochemical, and molecular information related to tumor metabolism, proliferation rate, invasiveness, and interaction with surrounding and remote areas—information that might be useful for clinical management. Especially, decisions on type and aggressiveness of treatment require detailed information on tumor type, location, and extent but also on biologic activity of the tumor and functional state of the surrounding brain. This comprehensive assessment of anatomic, functional, and molecular information is usually based on the spatial correlation of imaging data acquired sequentially with separate scanners, but the accuracy of this coregistration is limited by difficulties in patient repositioning and changes occurring between the different measurements. Sophisticated image fusion algorithms have been developed and are applied in many centers, but visual comparison of images positioned side by side is still the most commonly used approach in clinical practice. Temporal and spatial coregistration of morphologic and functional data in a single examination without repositioning the patient can be achieved by hybrid systems, as introduced with the PET/CT scanner (*1*). PET/CT is currently the most efficient imaging tool in general oncology, although PET and CT are still performed sequentially. Because the differentiation of soft-tissue contrast in the brain

Received Jan. 27, 2011; revision accepted Jul. 5, 2011.
For correspondence or reprints contact: Wolf-Dieter Heiss, Max Planck Institute for Neurological Research, Gleueler Strasse 50, 50931 Cologne, Germany.
E-mail: wdh@nf.mpg.de
Published online Aug. 12, 2011.
*Contributed equally to this work.

with CT is limited, a hybrid PET/MRI system will be better suited for applications in neurooncology. With such an integrated PET/MRI system, it is feasible to assess morphologic, functional, and molecular information on the human brain in a single session, in which several MRI procedures can be performed during a single PET study, for example, for ^{18}F-FDG (*2*). This review describes the value of the different imaging modalities in the various steps of the management of patients with brain tumors. Therefore, it is structured according to the questions arising in the clinical work-up.

DIAGNOSIS AND GRADING

For the diagnosis and classification of tumors of the nervous system, internationally accepted guidelines have been formulated (*3*), and for many of these tumors, grading is based primarily on histologic criteria, such as cell density, nuclear and cellular atypia, number of mitoses, and vascular endothelial proliferation. The system of the World Health Organization (WHO) classifies the most frequent brain tumors, the gliomas, into 4 grades (Table 1), with grades I and II being benign; grade III being anaplastic; and grade IV, glioblastoma multiforme, being the most malignant tumor with the worst prognosis (*4*). Histologic grading is based on tissue biopsies, which may not be representative since gliomas are frequently heterogeneous (*5*). Thus, imaging indicators of tumor grade and prognosis may be of additional value.

Morphologic Imaging

CT is often the first-line technique after the acute onset of new cerebral symptoms with a question of intracranial hemorrhage, ischemic stroke, or a space-occupying lesion. Tissue asymmetries or a change in tissue density, either decreased or increased, are diagnostic hints for space-occupying lesions. A slightly increased tissue density indicates an increase in tissue cellularity, whereas a strong increase of tumor density indicates tissue calcification, which can indicate a histologic primary brain tumor subtype such as an oligodendroglioma. A decreased tissue density indicates low tumor cellularity or edema. Contrast-enhanced CT can delineate a disrupted BBB, but its sensitivity is much lower than that of MRI. CT also has difficulties in the delineation of tumor borders or infiltration zones, and pathologies in the neighborhood of the skull base and the posterior fossa are better delineated by MRI because of the absence of artifacts caused by beam hardening in CT, in particular due to the petrous bone. CT has a clear advantage over MRI in its ability to show changes of bony structures that might be caused by tumors and additionally can detect calcifications in tumors, which are typically seen in oligodendrogliomas.

MRI is the major technique for the detection of the presence of brain tumors in patients, not only for the anatomic information that can be obtained through its high soft-tissue contrast and resolution but increasingly also for functional information.

Anatomic MRI relies on classic techniques such as T1- and T2-weighted imaging, fluid-attenuated inversion recovery sequences, and contrast-enhanced T1-weighted imaging (Fig. 1). Differential diagnosis relies on the location, size, and disruption of the BBB of a lesion, medical history, and age of the patient, although, among other limitations, disruption of the BBB does not allow for a reliable separation between low- and high-grade tumors (*6*) and about one third of nonenhancing gliomas are malignant (*7*).

Classic anatomic imaging is still the basis for diagnosis and grading but does not meet the requirements for individual cancer assessment before treatment or during follow-up (with the advent of modern cytostatic cancer therapies) or the trend toward individualized treatment.

PET

PET can overcome the limitations of conventional MRI and can be used to derive information on tumor hypoxia, necrosis, proliferative activity, or vasculature.

Glucose Metabolism. Glucose is the main substrate of the energy supply to the brain. The tracer for measurement of the cerebral metabolic rate of glucose is ^{18}F-FDG, which is transported into the tissue and phosphorylated to ^{18}F-FDG-phosphate but does not undergo significant further metabolism and accumulates in proportion to local metabolism. For calculation of quantitative metabolic rates, a conversion factor (lumped constant) is applied to account for the different properties of this analog tracer. Because of an overexpression of hexokinase II, this lumped constant is higher in tumors (*8*), and ^{18}F-FDG therefore overestimates the glucose consumption if the value for normal brain is used. This discrepancy between glucose consumption and ^{18}F-FDG uptake can be shown using ^{11}C-glucose and indicates that glucose consumption is not increased in certain gliomas despite a marked uptake of ^{18}F-FDG (*9*). Additionally, altered glucose transport into the tumor and increased non-

TABLE 1
WHO Classification of Gliomas

Parameter	Grade I	Grade II	Grade III	Grade IV
Tumor type	Low-grade astrocytoma	Low-grade astrocytoma	Anaplastic	Glioblastoma multiforme
Characteristic	Reserved primarily for pilocytic tumors	Diffuse infiltrating lesions with no enhancement	Variable enhancement with edema	Heterogeneous enhancement (often ring enhancement) with edema

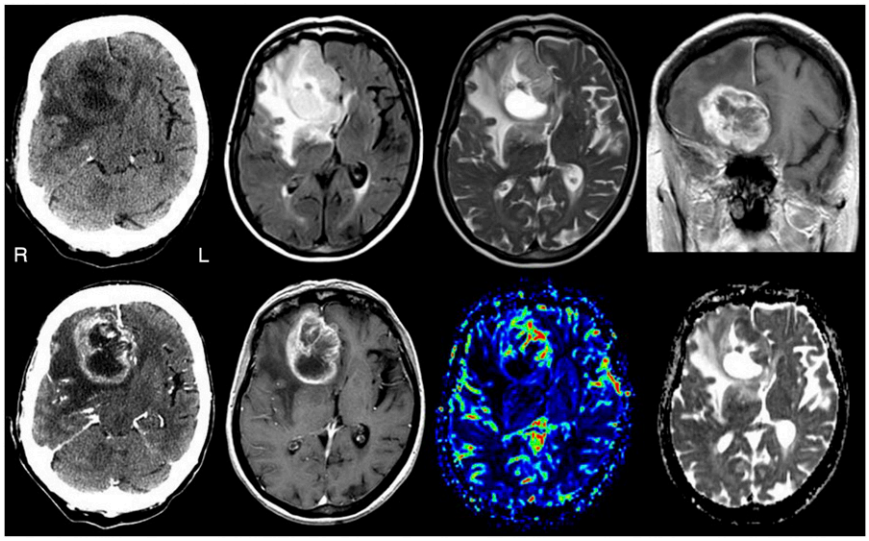

FIGURE 1. Images of patient with new onset of seizure and history of colon carcinoma. Top row from left to right shows CT scan, fluid-attenuated inversion recovery MR image, T2-weighted MR image, and T1-weighted contrast-enhanced MR image; bottom row from left to right shows contrast-enhanced CT scan, T1-weighted contrast-enhanced MR image, perfusion-weighted MR image (rCBV), and ADC image. T2-weighted image shows cortical involvement of tumor in anterior medial part, which is unusual for metastases. Perfusion-weighted image demonstrates rCBV elevation indicative of high-grade glioma. ADC values in more solid anteromedial parts are lower than in normal brain tissue, indicating higher cellularity. Final diagnosis was glioblastoma multiforme WHO IV.

oxidative glycolysis affect the calculation of cerebral metabolic rate of glucose; therefore, uptake of glucose relative to cerebral cortex or deep white matter is usually used for the identification of tumor tissue.

Imaging of brain tumors with ^{18}F-FDG was the first oncologic application of PET (*10*). As in other malignancies (*11*), glucose consumption is increased in brain tumors, especially in malignant gliomas, but differentiating tumors from normal tissue or nontumorous lesions is often difficult because of the high metabolism in normal cortex. ^{18}F-FDG uptake in low-grade tumors is usually similar to that in normal white matter, and uptake in high-grade tumors can be less than or similar to that in normal gray matter. The sensitivity of detection of lesions is further decreased by the high variance of ^{18}F-FDG uptake and its heterogeneity within a single tumor that has areas of low uptake and areas of high uptake near each other. Therefore, ^{18}F-FDG grading of newly discovered gliomas must be applied with caution, and the high variability must be taken into consideration. However, ratios of ^{18}F-FDG uptake in tumors to that in white matter (ratio of tumor to white matter > 1.5) or gray matter (ratio of tumor to gray matter > 0.6) were able to identify and distinguish benign tumors (grades I and II) from malignant tumors (grades III and IV) (Fig. 2) (*12*). Delayed imaging (3–8 h after injection) can improve the distinction between tumor and normal gray matter (*13*), since excretion of the tracer is faster in normal brain than in tumor tissue.

The amount of accumulation of ^{18}F-FDG in a primary brain tumor correlates with histologic tumor grade (*14,15*), cell density (*16*), and survival (*17,18*). Glucose consumption in normal brain tissue is reduced in most patients with malignant brain tumors (*19*). The impairment of tissue metabolism is related to prognosis (*20*). The most malignant gliomas (grade IV, glioblastoma) show high uptake that is often heterogeneous because of the necroses typical of this tumor type. Relatively benign tumors with high ^{18}F-FDG uptake include pilocytic astrocytoma, which is characterized by metabolically active fenestrated endothelial cells, and ganglioglioma. In meningiomas, ^{18}F-FDG uptake is variable and may be related to aggressiveness and the probability of recurrence (*21*). Other malignant tumors in the brain—primitive neuroectodermal tumors, medulloblastomas, malignant lymphomas, and brain metastases from systemic cancers—often show high ^{18}F-FDG uptake (*22,23*).

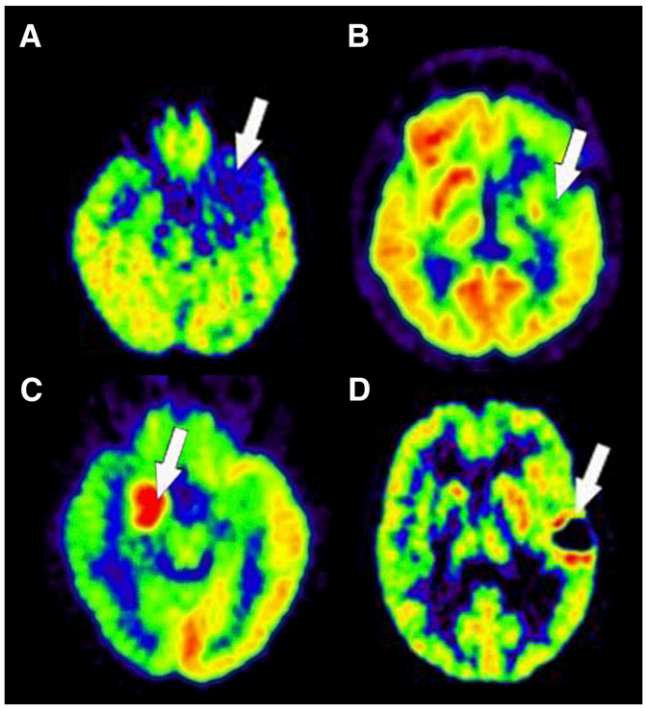

FIGURE 2. Typical PET patterns of ^{18}F-FDG uptake in gliomas of different grades: metabolic activity of grade II glioma is below level of gray matter (A); that of grade III and IV gliomas is above (B and D). Typical of glioblastoma (grade IV) is central necrosis and metabolically active rim (arrows). Oligodendrogliomas (C) have higher metabolic activity than astrocytomas of same grade (higher cellular density).

For the interpretation of ^{18}F-FDG brain scans, the similarity of ^{18}F-FDG uptake of tumor and cortex is a limiting factor, which is especially critical for small lesions. Because of the limited spatial resolution of PET and partial-volume averaging, ^{18}F-FDG uptake can be underestimated in small lesions. ^{18}F-FDG uptake in brain tumors is assessed best if coregistration with MRI permits reliable localization of PET data.

Amino Acid Uptake. Labeled amino acids and their analogs—L-[methyl-^{11}C]-methionine (^{11}C-MET), ^{11}C-tyrosine, ^{18}F-fluorotyrosine, ^{18}F-deoxyphenylalanine (F-DOPA) and *O*-2^{18}F-fluoroethyltyrosine—are particularly attractive for imaging brain tumors because of the high uptake in tumor tissue and low uptake in normal brain and, as a consequence, higher tumor–to–normal-tissue contrast. This increased amino acid uptake, especially in gliomas, is not a direct measure of protein synthesis or dependent on BBB breakdown but rather is related to increased transport mediated by type L amino acid carriers: facilitated transport is upregulated because tumors increase transporter expression in their vasculature (*24*). Additionally, the countertransport system A is overexpressed in neoplastic cells and seems to be positively correlated with the rate of tumor cell growth (*25*). Therefore, elevated transport of amino acids not only is a result of increased protein synthesis but also reflects the increased demand for the different metabolic activities in the tumor cell. Tumors also influence growth of their vasculature and therefore can regulate their increased demand for nutrients, including amino acids.

The most frequently used radiolabeled amino acid, ^{11}C-MET, can be applied only in centers with an on-site cyclotron. For the discrimination of brain tumors from nontumoral lesions, a sensitivity of 76% and a specificity of 87% (*26*) have been described. In gliomas, ^{11}C-MET uptake is greater in high-grade than in low-grade tumors (Fig. 3) (*27–29*) and is increased in most low-grade gliomas in the absence of BBB damage—a substantial advantage over CT, conventional MRI, and ^{18}F-FDG PET (*30,31*). Therefore, ^{11}C-MET can provide additional information when used in combination with ^{18}F-FDG PET for diagnosis of these tumors. Angiogenesis and amino acid uptake are related (*32*). In many instances, the extent of increased ^{11}C-MET uptake is larger than that of contrast enhancement (*33*) and indicates tumor infiltration and tumor margins. Especially in low-grade gliomas, amino acid uptake is related to prognosis and survival (*34,35*). ^{11}C-MET PET therefore has special value in low-grade gliomas: for differentiation from nontumorous lesions, for detection of recurrences, for indicating changes in grade of progressing disease, and for potentially allowing a better prediction of prognosis. ^{11}C-MET PET was useful for differentiating tumorous from nontumorous lesions in children and young adults when the decision about further therapy was difficult or impossible to make from routine structural imaging alone (*36*). High ^{18}F-fluoroethyl-L-tyrosine (FET) uptake indicative of tumor cell infiltration was associated with markers of neuronal cell loss in ^{1}H MRS (*37*).

^{11}C-MET uptake differs with tumor type: in oligodendrogliomas, uptake tends to be higher than in astrocytomas of the same histologic grade, although oligodendrogliomas are less aggressive (*38*). In oligodendrogliomas, ^{11}C-choline PET may be useful in evaluating the potential malignancy, but ^{11}C-MET PET is superior in detecting hot lesions (*39*). ^{11}C-MET uptake is increased in other malignant intracranial tumors but also in benign neoplasias such as meningiomas (*22*).

Because of the short half-life of ^{11}C (20 min) ^{18}F-labeled aromatic amino acid analogs have been developed for tumor imaging. Tumor uptake of ^{18}F-FET and dihydroxy-^{18}F-fluoro-L-phenylalanine (F-DOPA) is similar to that of ^{11}C-MET (*40,41*). In a large study, F-DOPA demonstrated excellent visualization of high- and low-grade tumors and was more sensitive and specific than ^{18}F-FDG, but no significant relation to tumor grade or to contrast enhancement was observed (*42*). Especially in newly diagnosed tumors, uptake was related to proliferation, whereas this correlation was not observed in recurrent gliomas (*43*).

Nucleoside Uptake. Labeled nucleosides are indicators of cellular proliferation and should provide information on histologic grade. The thymidine analog 3-deoxy-3-^{18}F-fluorothymidine (^{18}F-FLT) was developed as a noninvasive tracer of tumor cell proliferation (*44*). Uptake of ^{18}F-FLT correlates with thymidine kinase-1 activity, an enzyme expressed during the DNA synthesis phase of the cell cycle (*45*), which is high in proliferating cells and low in quiescent cells. With this tracer, an excellent delineation of grade III and IV tumors with a high tumor-to-normal ratio was obtained

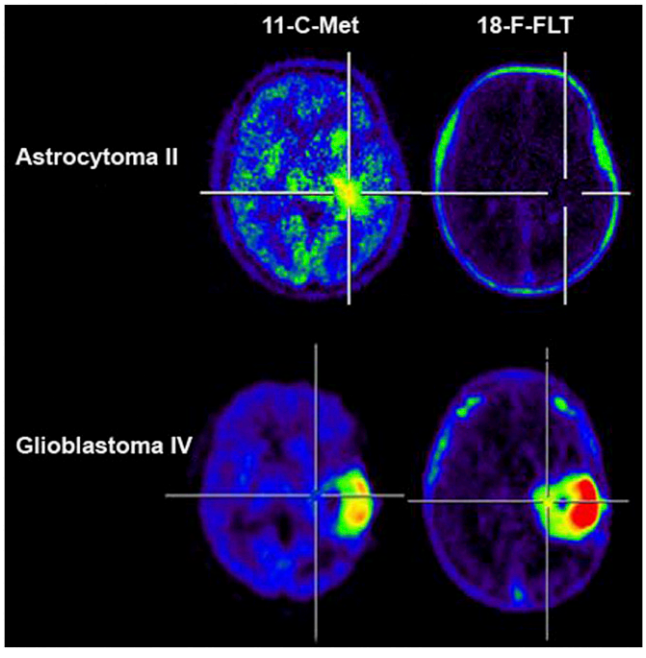

FIGURE 3. PET images showing uptake of ^{11}C-MET and of ^{18}F-FLT in gliomas of low grade (top row) and high grade (bottom row). Uptake of ^{18}F-FLT is especially high in malignant glioma and also demonstrates infiltration into surrounding tissue.

(*46*), whereas grade II gliomas and stable lesions did not show considerable tracer uptake (Fig. 3); additionally, a high correlation of ^{18}F-FLT uptake was seen with Ki-67 expression as a surrogate marker for tumor proliferation (*47*). Although absolute tumor uptake of ^{18}F-FLT was lower than that of ^{11}C-MET, tumor–to–normal-brain uptake ratios were higher than for ^{11}C-MET because of the low ^{18}F-FLT concentration in normal brain. Gadolinium-enhanced MRI yields complementary information on tumor extent, because ^{18}F-FLT uptake also occurs in regions with a disrupted BBB and sensitivity for detection of low-grade gliomas is lower than with ^{11}C-MET (*48*). A kinetic analysis of ^{18}F-FLT uptake permits the assessment of tumor proliferation rates in high-grade gliomas, whereas uptake ratios of ^{11}C-MET and ^{18}F-FLT failed to correlate with the in vitro–determined proliferation index by Ki-67 immunostaining (*46*). In another study (*49*), ^{18}F-FLT PET was superior to ^{11}C-MET PET in tumor grading and assessment of proliferation in different gliomas, and the combination with ^{11}C-MET PET added significant information.

Marker of Hypoxia. Hypoxia in tumors is a consequence of disturbed angiogenesis not balanced to the needs of the quickly proliferating tissue. As a consequence, oxygen supply is inadequate. ^{18}F-fluoromisonidazole (^{18}F-FMISO) is a marker of hypoxia and has potential for detecting a specific pathophysiology of brain tumors (*50*). ^{18}F-FMISO-PET demonstrated a correlation with perfusion at 0–5 min after injection, whereas late persistent uptake of this tracer was independent of perfusion and BBB disruptions (*51*). Hypoxia is a driving force for angiogenesis, as also expressed in a correlation between ^{18}F-FMISO uptake and Ki-67 and vascular endothelial growth factor (VEGF) receptor 1 expression (*52*), and considerable ^{18}F-FMISO uptake was therefore found in high-grade but not in low-grade gliomas. The volume of hypoxia in a glioma as determined by ^{18}F-FMISO uptake before initiation of treatment was related to aggressiveness as assessed by serial MRI (*53*) and to progression and survival after radiotherapy (*54*).

Somatostatin Receptor Ligands. Meningiomas express somastatin receptors of subtype 2, which can be detected by ^{68}Ga-DOTA-phenyl-tyrosin-osteotide. In contrast to ^{18}F-FDG, ^{68}Ga-DOTATOC shows a high meningioma-to-background ratio (*55*) and was helpful in visualizing the location and extent of meningiomas near bony structures, especially at the base of the skull. This tracer was especially successful in improving volume delineation for planning intensity-modulated radiation therapy in combination with CT (*56,57*) and recently with simultaneous MRI (*58*)

Physiologic MRI

Modern MRI techniques are being increasingly used to improve the sensitivity and specificity of tumor diagnostics; these techniques offer possibilities for the detection of functional information. MRS can assess tumor metabolism and physiology, DWI can assess tissue microstructure by characterizing water mobility, and perfusion-weighted imaging can assess vascular integrity and function.

MRS. MRI is primarily based on the imaging of hydrogen atoms contained in water and fat. MRS is based on the detection of molecule-specific energy spectra, which are dependent on the chemical molecular structure and can be interpreted as a fingerprint of the specific molecule. Such a spectrum is represented by a curve, with the area under the curve of a certain peak representing the concentration of the metabolite within the sampled tissue, and the position of the peak, which is shifted away from the position of a standard substance, representing the metabolite. The amount of the shift is counted in parts per million and referred to a standard substance at 0 ppm by definition.

Single-voxel spectroscopy gives information just from a certain tissue area, whereas 2- and 3-dimensional chemical shift imaging collect data from one or more tissue slices with several voxels in each slice. Multivoxel chemical shift imaging can therefore better delineate tissue inhomogeneities than single-voxel spectroscopy.

Absolute quantification of metabolites is difficult; therefore, relative quantification methods are usually used for clinical purposes. Metabolite data can be referred to other metabolites within the same voxel, but since all the metabolites can be changed by a tumor, it is advisable to relate tumor data to contralateral healthy tissue.

Several metabolites can be measured by MRS; because of the relaxation time, the amount of assessable metabolites is dependent on the echo time of the sequence used.

The main metabolites for tumor diagnostics are shown in Table 2.

The separation of low-grade and high-grade gliomas is of high prognostic importance. Choline and lipids have shown the best predictive value; by the use of MRS, tumors could be correctly diagnosed 85%–95% of the time (*59,60*). In general, brain tumors tend to differ from nonneoplastic tissue by an elevation of choline and possibly lactate and lipids, combined with a reduction of tumor creatine or tumor *N*-acetylaspartate (NAA). Actively proliferating tumors require an increased membrane turnover leading to a choline increase. Because of destruction of neurons by the tumor, NAA is decreased (Fig. 4); lactate indicates anaerobic glycolysis by the tumor tissue, and lipids indicate necrosis.

For tumor grading, lactate and lipids indicate higher tumor grades (*61*), as does increased choline (Fig. 5)] (*62*). Choline as part of cell membrane phospholipids correlates well with the Ki-67 proliferation marker in gliomas (*62,63*). A cutoff of 1.6 for normalized choline values was found to be predictive of high-grade astrocytomas. Elevated choline is unfortunately not completely specific for high-grade tumors, since pilocytic astrocytomas (*64*) and low-grade oligodendrogliomas can have increased choline levels as well. For oligodendrogliomas, a cutoff of 2 was indicated by Xu et al. for the separation between low- and high-grade oligodendrogliomas (*65*). Elevated normalized creatine values indicate a shorter time to progression in WHO grade II and III astrocytomas (*66,67*).

TABLE 2
Main Metabolites Detected by MRS, Their Chemical Shift Position, and Interpretation

Metabolite	Peak position (ppm)	Echo time used	Interpretation	Found in normal tissue?
Choline	3.2	Short and long	Membrane turnover	Yes
Creatine/phosphocreatine	3.02, 3.8	Short and long	Energy metabolism	Yes
NAA	2.01, 2.6	Short and long	Neural tissue integrity	Yes
Lipids	0–2	Short and long	Tissue necrosis	Only as contamination
Lactate	1.33	Short and long	Anaerobic glycolysis	No
Taurine	3.36	Short	Pediatric tumors	Below sensitivity
Myoinositol	3.56, 4.06	Short	Glial activation	Yes

Clinically used echo times are 20–30 ms (short), 135–144 ms (long), or 270 ms.

Because tumor tissue is known to be heterogeneous, MRS can also be used to guide stereotactic brain biopsies to assess the region with the highest membrane turnover (*68,69*), but this is still the domain of PET with ^{18}F-FDG or amino acids.

MRS can also be used to assess infiltrating brain tumors, since choline elevation can extend to areas without contrast enhancement or to tissue that appears normal on conventional MRI. An increase of myoinositol indicates zones of active glial activation due to a reaction toward infiltrating tumor cells (*70*), as does the choline/NAA index (*71*).

MRS can aid in the differential diagnosis of brain tumors. About two thirds of meningiomas show an alanine resonance at 1.5 ppm, which is specific for meningiomas. Metastases tend to have low NAA resonances while showing a high lipid peak, and choline can be elevated. Metabolite concentrations in the peritumoral region can help in differentiating glioblastomas from metastases and lymphomas (*72*).

MRS can also image other nuclei besides protons. One of these so-called X-nuclei is ^{13}C, enabling the use of ^{13}C-labeled agents such as ^{13}C-pyruvate for imaging. Hyperpolarized ^{13}C-pyruvate was used during radiotherapy in an animal model of glioma tumor and showed a reduction of ^{13}C-lactate production within 72 h of radiotherapy (*73*). In a lymphoma model, this technique of evaluating the pyruvate–lactate flux showed results comparable to those of ^{18}F-FDG PET during chemotherapy (*74*). This technique offers new possibilities for assessing physiologic and pathophysiologic changes in tumors noninvasively, but the technique is experimental and not available for clinical use yet. In addition, hyperpolarization is technically difficult to achieve, and the short half-life of the hyperpolarized state also limits the applicability of the technique.

DWI. DWI is a probing of the microscopic motion of water molecules within tissue; this motion is driven by temperature, following the Brownian law, and is influenced by tissue structure (*75*). Infiltration of healthy brain by tumorous tissue causes alterations of water diffusion assessable by DWI (Fig. 1). An increase in cellular density, reduction of extracellular space, and increase in viscosity, for example, generate a decrease of Brownian motion of water molecules and a decrease of the calculated and (commonly accepted as a measure of water diffusion) apparent diffu-

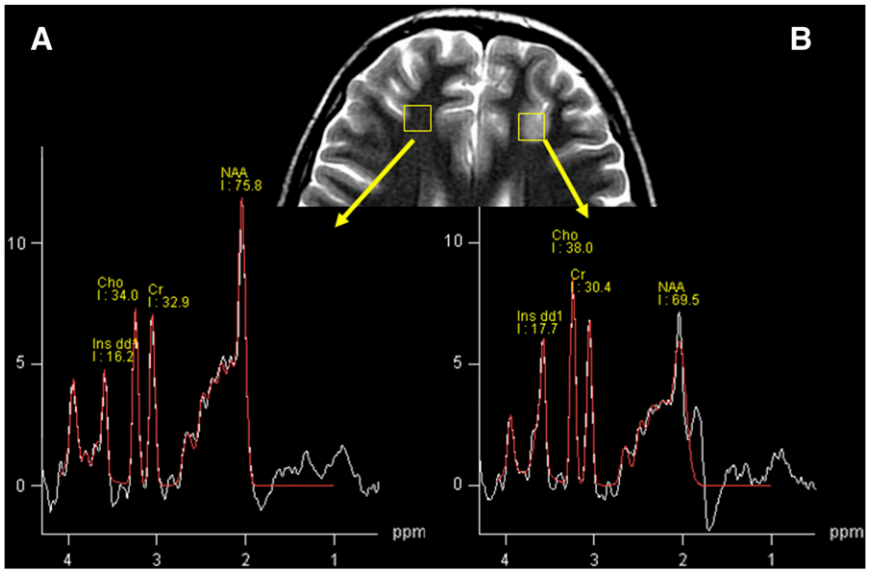

FIGURE 4. Patient with new seizure onset and small left frontal signal elevation on T2-weighted MRI. ^{1}H-MR spectroscopy (echo time, 30 ms; repetition time, 1,500 ms; 2-dimensional chemical shift imaging) shows normal spectrum on right side (A) and slight choline elevation with NAA reduction of lesion on left side (B). Low-grade glioma was found on stereotactic biopsy. Red line represents curve fit of analysis software; area under curve, which corresponds to metabolite concentrations, is given by numbers at peaks. Ins = inositol; Cho = choline; Cr = creatine; NAA = *N*-acetylaspartate.

sion coefficient (ADC, mm^2/s). ADC values are quantifiable and quickly measurable with a suitable resolution. Low values in ADC maps of solid gliomas are correlated with a higher grade (*76*). But, as a limitation, coexistent edema may superimpose measurements of ADC values, resulting in a decreased accuracy in separation of low- and high-grade gliomas. In children, medulloblastomas and atypical rhabdoid-teratoid tumors of the posterior fossa show significantly lower ADC values than do ependymomas and pilocytic astrocytomas (*77,78*). Central neurocytomas also show low ADC values (*79*).

Of special interest are more sophisticated higher-order diffusion techniques such as diffusion kurtosis imaging, enabling a more profound characterization of microstructural changes (*80*). First results are promising regarding grading and differential diagnosis of brain tumors (*81*).

Perfusion-Weighted Imaging. In comparison to healthy brain tissue, high-grade gliomas develop an increased macro- and microvasculature. The relative cerebral blood volume (rCBV) is increased, predominantly as a result, and correlates with aggressive tumor growth (Fig. 1).

At present, the preferred technique to measure brain perfusion is tracking of a well-defined bolus of contrast medium with a dynamic MRI sequence sensitive to T2* effects. The area under the signal curve] is an estimate of rCBV. Extravasations of contrast medium caused by disruption of the BBB affect the calculation of rCBV in high-grade gliomas and have to be adjusted for by sophisticated mathematic models (*82*). The application of a preloading dose of contrast medium is another possibility to minimize the effects of leakage (*83,84*). The increase of permeability in capillaries of high-grade gliomas can be estimated by dynamic T1-weighted contrast-enhanced MRI. Of special interest is the so-called transport constant (*85*), which describes the exchange of contrast medium from intra- to extravascular space. The transport constant is a quantifiable value and can be calculated on the basis of compartmental model estimations. This technique is quite complex and has been available so far only in advanced imaging centers.

Cao et al. proposed a special short T2*-weighted MRI sequence measuring perfusion parameters and permeability at the same time (*86*). Careful interpretation of data achieved by T1- or T2*-based MRI techniques is mandatory during therapy with corticosteroids or VEGF-specific antibodies (see the section on monitoring treatment effects

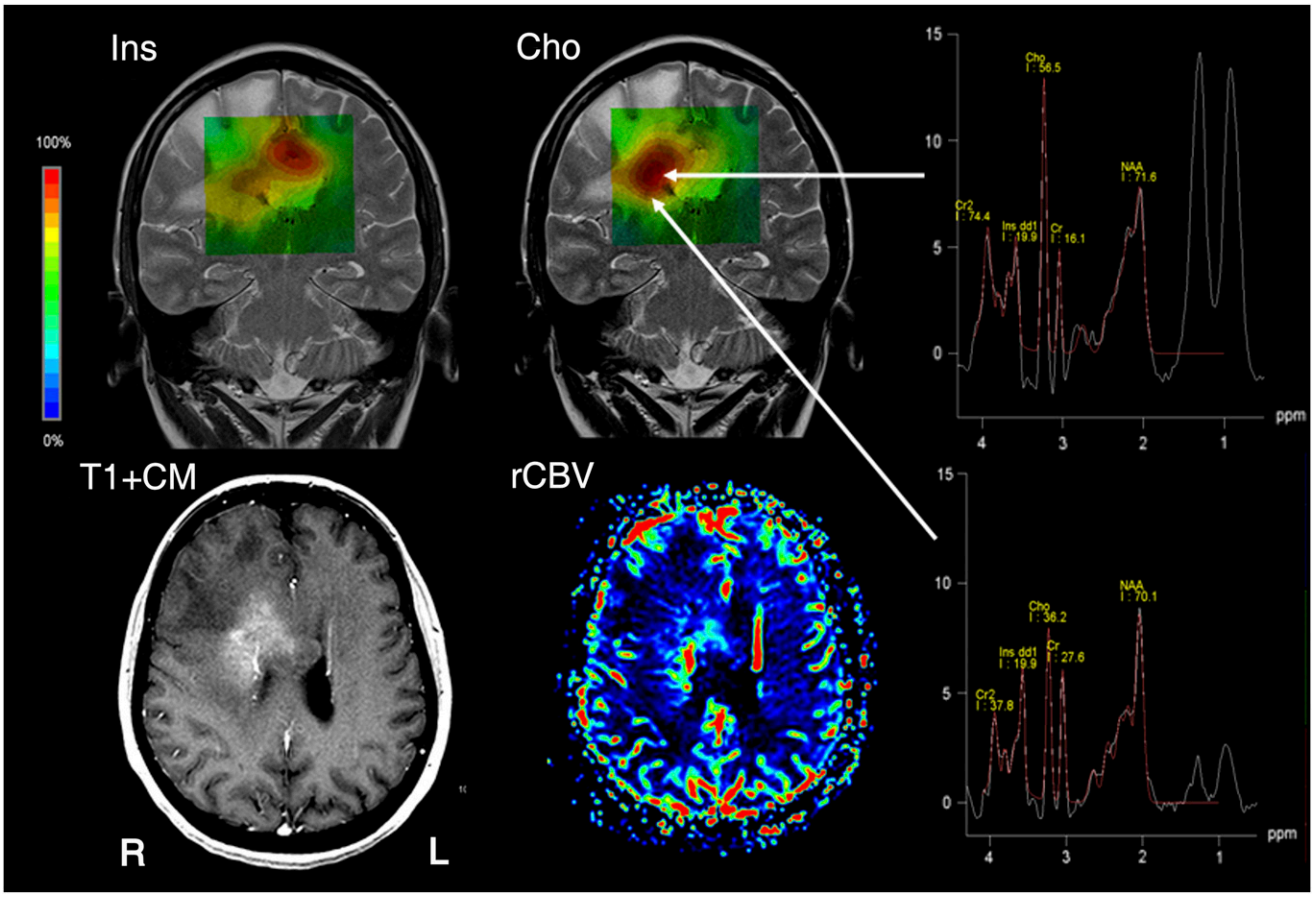

FIGURE 5. Patient with headache and no neurologic deficit despite paresthesia of left arm. At top, MRI metabolite maps of inositol (Ins) and choline (Cho) show inhomogeneity of high-grade glioma. At bottom, disrupted BBB is demonstrated by T1-weighted contrast-enhanced MR image (T1+CM), elevation of rCBV in same area. Spectra from area with highest choline elevation contain lipid resonances indicating necrosis (arrows).

with MRI). T2*-weighted perfusion techniques are widely available, but as a shortcoming the results are barely comparable because of a lack of standardized protocols and different postprocessing algorithms dependent on the manufacturers of MRI devices or third-party software packages. Only large and solid parts of a glioma should be evaluated, and because of the limitations mentioned before, identical postprocessing parameters have to be applied to detect local dedifferentiation of gliomas or therapeutic effects by radiochemotherapy.

Perfusion-weighted imaging data can be used for tumor grading, since high-grade tumors tend to show higher rCBV values (*87–89*) than does normal-appearing contralateral tissue. Law et al. found a threshold of 1.75 for determining a high-grade glioma (*87*). Oligodendrogliomas differ from astrocytomas with respect to their rCBV cutoff for the difference between low and high grade. This cutoff tends to be higher for oligodendrogliomas, at a ratio of about 2.14 (*90*).

Higher-grade gliomas also tend to show higher capillary leakage, although the correlation with grading was found to be weaker than for rCBV measurements (*91,92*).

Blood Oxygen Level–Dependent and T2′ Imaging. Blood oxygen level–dependent imaging refers to the contrast effect between oxygenated and deoxygenated hemoglobin. Deoxygenated hemoglobin does have a paramagnetic effect and causes a slight signal loss in susceptibility sensitive sequences (T2*, echo-planar imaging), whereas oxygenated hemoglobin has diamagnetic characteristics with no signal loss in these sequences. This blood oxygen level–dependent effect is the technical basis of functional MRI, as well as for parts of susceptibility weighting and T2′ imaging. Low T2′ values are thought to represent areas with high oxygen consumption or high oxygen extraction fraction (*93,94*). The T2′ values can be influenced by confounding factors such as microcalcifications, hemorrhage, and microvasculature. Saitta et al. (*93*) found a significant T2′ difference between low- and high-grade gliomas; high-grade gliomas showed lower T2′ values indicating higher oxygen extraction, possibly caused by a higher metabolic state.

Imaging of Tumor Inhomogeneities

A specific and important application of PET tracers is the detection of especially active compartments in a tumor or of residual tumor after resection. Gliomas are often heterogeneous and may contain regions of different histologic grades. The areas of higher malignancy might not show contrast enhancement on conventional MRI or CT, but they define the prognosis and must be included in the material sampled for diagnosis in biopsy. Stereotactic biopsy based on coregistered ^{18}F-FDG PET and MRI therefore improved the assessment of tumor grade (*95*). Chemical shift spectroscopic imaging can also be used for guidance of stereotactic biopsies (*69*) based on choline information that indicates areas with higher cell membrane turnover. In a comparison of ^{11}C-MET PET and 2-dimensional chemical shift imaging, the spectroscopic technique could even show tumor areas of increased proliferation rate when PET showed negative or nonspecific tracer uptake while the maximum changes in both techniques correlated well (*96*). Perfusion-weighted imaging data can also be used to characterize spatial heterogeneity in high-grade gliomas (*97*).

With regard to tumor extent and infiltration into surrounding tissue, assessment of ^{11}C-MET uptake is superior to measurement of glucose consumption (*98,99*) and to conventional contrast-enhanced MRI (*100,101*) or MRS (*102*), and ^{11}C-MET PET detects solid parts of tumors as well as the infiltration zone with high sensitivity and specificity (*103*).

EFFECTS ON SURROUNDING AND REMOTE BRAIN AREAS

PET

Brain tumors are often space-occupying and infiltrating lesions and therefore affect the surrounding tissue but also remote brain areas. Especially in malignant tumors, there is a wide rim of reduced glucose metabolism that might be partly due to edema formation and to functional inactivation by the infiltrating tumor (*19*). This impairment of glucose metabolism in the brain outside the tumor is related to prognosis (*20*). Patients with brain tumors have decreased metabolism in the contralateral cortex, and the degree of decrease correlates with tumor size. This phenomenon may partly be caused by corticosteroids, but a functional inactivation of the contralateral hemisphere cannot be excluded (*104*), and this inactivation is also observed in the contralateral cerebellum.

The function of the brain outside the tumor and the effect of the lesion on eloquent areas can be studied by functional imaging such as activation PET or functional MRI. ^{15}O-water is the most frequently used cerebral blood flow tracer for this purpose, allowing up to 12 measurements under different conditions, but ^{18}F-FDG has also been used to record functional changes. Coregistration and fusion image display with 3-dimensional MRI are necessary for accurate anatomic localization (*105*). The location of functionally activated areas may be altered by several effects of the tumor: the new mass can displace the primary cortical centers, infiltrations can reduce the activation and impair the function of a specific area, or functional activations can occur at atypical locations, even in the contralateral hemisphere, as an indication of the reorganization of functional networks (*106*). Exact localization of eloquent areas is an important clinical goal for planning tailored surgery, and infiltrated tissue may sometimes still be functional.

Motor activity usually leads to significant activation in respective areas of contralateral motor cortex, in the supplementary motor area, and in the ipsilateral cerebellum. In patients with brain tumors, functionally activated areas along the precentral gyrus that exceed displacement due to mass effects have been observed. When cortical lesions causing contralateral spastic paresis abolish activation of motor cortex, more intense activation of secondary motor areas and of motor cortex ipsilateral to the paretic limbs is observed (*107*).

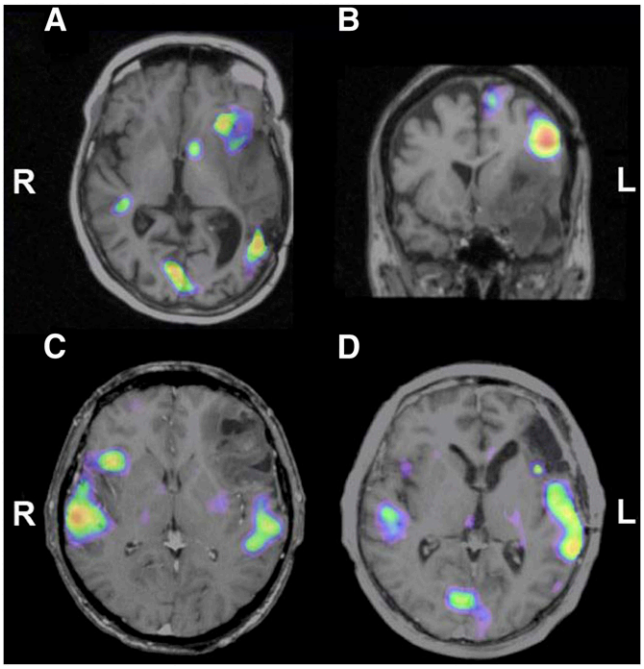

FIGURE 6. Activation of $H_2{}^{15}O$ PET by verb generation, coregistered to MRI. In patient at top, with left temporal glioma, Broca region is rostral (A) and motoric speech region is dorsal (B). Alternatively, in patient at bottom, with grade III astrocytoma, Broca region is transferred to contralateral homotopic area (C), and this activation of nondominant hemisphere is reversible (D).

The functional activation of language is lateralized to the left hemisphere in most right-handers, whereas in left-handers it may be represented in either hemisphere or even bilaterally (*108*). The localization of sensory and motor language areas is of interest for surgical planning in patients with tumors in inferior frontal and temporoparietal areas. Active semantic or language production tasks provide clearly lateralized activations, in particular in the inferior frontal cortex of the dominant hemisphere, in the superior temporal cortex, in the anterior cingulated cortex and the adjacent supplementary language area, and in the contralateral cerebellum. In patients with brain tumors in the dominant hemisphere, a considerable reorganization of the language-related network is observed (*109*), dependent on the speed of the development of the brain lesion: a verb generation paradigm increased the activation area beyond the primary language regions to the left frontal medial gyrus, the orbital inferior frontal gyrus, the anterior insula, and the left cerebellum (Figs. 6A and 6B). Unlike the healthy volunteers, two thirds of the right-handed patients also showed activation of the right inferior frontal gyrus, the area homologous to the Broca area (Fig. 6C). In 18% of patients, a reversed dominance was observed (*110*); successful resection of a left frontotemporal tumor improved aphasia and restored left hemisphere dominance, suggesting a reversible disinhibition by removal of the primary functional damage (Fig. 6D). These studies support a hierarchical organization of the language network for speech performance and recovery and stress the importance of left-sided areas around the primary language centers; contralateral areas activated by reduced transcallosal inhibition can only partially compensate for damage of left-sided centers (*106,111*). The hierarchy of the functional network in an individual patient should be considered in planning surgical interventions.

MRI

Morphologic imaging does show signs of edema and mass effect. Functional or physiologic imaging, such as functional MRI using the blood oxygen level–dependent effect, can be applied to demonstrate eloquent brain areas before surgery as well as functional plasticity of the brain after therapy. Functional MRI data can easily be referenced to 3-dimensional anatomic datasets for neuronavigational purposes, since functional data and anatomic data are acquired within the same session without patient repositioning. Language examinations and motor tasks for functional MRI can be performed within 20–30 min, and language functional MRI has replaced the Wada test for probing of language lateralization (*112*). Diffusion tensor imaging, a DWI technique applying mathematic models to calculate and visualize white matter tracts, can show displacement or disruption of fiber tracts caused by a brain tumor (Fig. 7). This information can help the neurosurgeon to plan and guide an approach to a tumor and the resection.

DWI has also been used to delineate tumor margins. Compared with the lower fractional anisotropy values of the tissue around metastases, higher peritumoral fractional anisotropy, a marker of directed diffusion of water molecules, indicates peritumoral spread of neoplastic cells (*113*).

PROGNOSIS

PET

In most patients with malignant brain tumors, glucose consumption in the surrounding brain is reduced, and this reduction correlates with prognosis (*20*). Especially in low-grade gliomas, amino acid uptake is related to prognosis and survival (*34,35*).

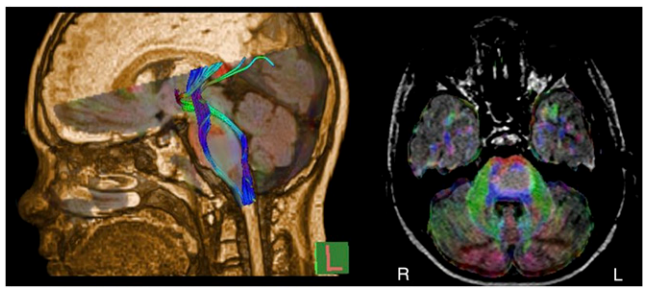

FIGURE 7. Diffusion tensor MRI demonstrates displaced and not destroyed/infiltrated pontine longitudinal fiber tracts. Fibers are displaced anteriorly and posteriorly by left-sided pontine glioma. Color coding indicates fiber direction: red = left/right; blue = cranial/caudal; green = anterior/posterior.

MRI

Morphologic imaging can indicate tumor progression by increasing mass effect and increasing areas of elevated T2 signal intensities, as well as increasing or new contrast enhancement in untreated brain tumors. Prognostic information can be derived only by physiologic imaging techniques.

In untreated low-grade brain tumors, an elevated rCBV (*114,115*) or a near-normal or elevated creatine level (*66*) indicate a short progression-free survival time and poorer prognosis. rCBV elevations can precede malignant transformation and new contrast enhancement by up to 12 mo (*116*). In children, the percentage change of choline or NAA combined with perfusion measurements in serial MRI examinations was found to be useful in predicting tumor progression (*117*). Before antiangiogenic therapy, ADC analysis of gliomas tended to predict progression-free survival in recurrent glioblastoma multiforme patients (*118*).

MONITORING TREATMENT EFFECTS

PET

Because of the high cortical background activity, ^{18}F-FDG is limited in the detection of residual tumor after therapy (*119*). The effects of radiation and chemotherapy can be shown only after a few weeks of treatment (*120*), and recurrent tumor or malignant transformation is marked by newly occurring hypermetabolism (*121*). Hypermetabolism after radiotherapy, however, can also be mimicked by infiltration of macrophages. With these limitations, ^{18}F-FDG PET is not the preferred method for the assessment of therapeutic effects (*122*). For this application, amino acid and nucleoid tracers are better suited (*123–127*). Several studies suggested that outcomes are better for patients in whom ^{11}C-MET or ^{18}F-FET PET coregistered to MRI are applied for treatment planning and follow-up than for patients diagnosed by MRI alone (*123–126,128*). In the follow-up and for the management of patients with brain tumor, the differentiation between recurrent tumor as a sign of treatment failure and necrosis as an indicator of success is essential. For that application, ^{11}C-MET PET coregistered to MRI has high sensitivity and specificity (~75%) (*129–132*). Malignant progression in nontreated and treated patients was detected with high sensitivity and specificity by ^{11}C-MET PET (Fig. 8). The increase in ^{11}C-MET uptake during malignant progression was also reflected by an increase in angiogenesis-promoting markers such as VEGF (*133*). The volume of metabolically active tumor in recurrent glioblastoma multiforme was underestimated by gadolinium–diethylenetriaminepentaacetic acid–enhanced MRI (*134*). The additional information supplied by ^{11}C-MET PET changed management in half the cases (*135*).

Responses after chemotherapy can be detected by amino acid PET early in the course (*136–138*), suggesting that deactivation of amino acid transport is an early sign of response to chemotherapy. ^{18}F-FET PET coregistered to MRI detected the effects of a multimodal treatment more sensitively than did conventional MRI alone (*139*) and reached a sensitivity of more than 80% and a specificity of close to 100% (*140*). With ^{18}F-FLT PET, a distinction between responders and nonresponders to a combination therapy was possible: ^{18}F-FLT PET at 2 and 6 wk predicted survival better than did MRI (*141*). Multimodal imaging, including various PET and MRI modalities, will have a great impact on the development of new therapeutic strategies, such as targeting to proliferating cells (*142*) or applying gene therapy vectors (*143*).

MRI

Classic MRI techniques are still the basis for follow-up studies, but after modern therapies such as combined radiochemotherapy or antiangiogenic therapy, the so-called pseudoprogression and pseudoresponse limit the usefulness of the classic McDonald criteria (*144,145*) during early follow-up examinations. Therefore, physiologic MRI might be helpful in these situations.

Monitoring of response to radiochemotherapy by ADC measurements can be recommended because changes in proton diffusion during the first weeks after onset of therapy are indicators of the intended antitumorous effect and therefore a prognostic marker for sufficient response to radiochemotherapy (*146,147*). In addition, DWI values of gliomas before treatment correlated with the probability of response to therapy with bevacizumab in a study performed by Pope et al. (*118*). Functional diffusion maps show promise as a way of providing an early surrogate marker for

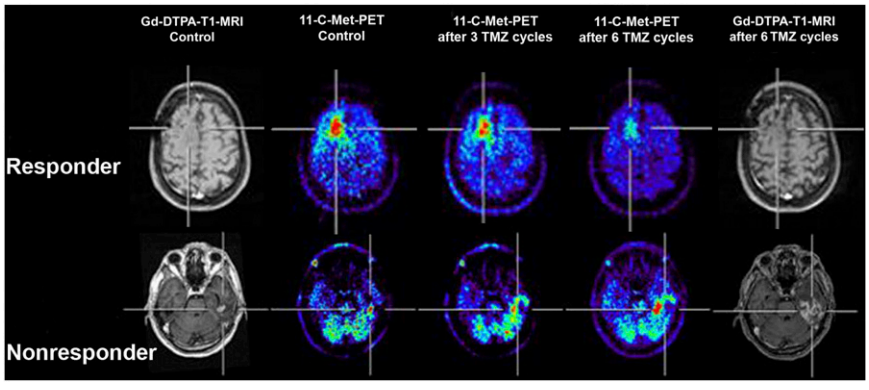

FIGURE 8. Decrease of ^{11}C-MET uptake on PET demonstrates response to chemotherapy and favorable prognosis, whereas increase in amino acid uptake is related to no response to chemotherapy and unfavorable outcome. Gd-DTPA = gadolinium–diethylenetriaminepentaacetic acid; TMZ = temozolomide.

treatment response as well (*146,148,149*). During radiotherapy, early changes of rCBV can indicate response to treatment and correlate with survival (*150*). Especially, the use of voxel-by-voxel parametric response maps at 3 wk after radiotherapy can help to predict overall survival (*151*).

Anti-VEGF chemotherapy leads to new problems in assessing tumor response using conventional MRI. The contrast enhancement as the major factor of the McDonald criteria cannot be used since the therapy leads to a marked reduction of BBB disruption. In solid gliomas, this therapy may induce lesions resembling ischemic brain, with high DWI and low ADC values (*152,153*). Nevertheless, changes in ADC histogram analysis may be predictive of response in the anti-VEGF treatment of recurrent high-grade gliomas (*154*). It has been observed that primary brain tumors might change their behavior under anti-VEGF therapy from a necrotizing growth to a more infiltrative growth, which can best be observed on fluid-attenuated inversion recovery images (*155*).

RESIDUAL TUMOR AND RECURRENCES

PET

The capacity of PET to identify tumor compartments that differ in activity is especially important for the detection of residual or recurrent tumor after resection and for differentiation between treatment-induced changes such as necrosis and active proliferating tissue. Actually, in individual cases, necrotic and active tissue can be found next to each other or may even overlap (*156*), and ^{18}F-FDG in macrophages that infiltrate tissue after radiotherapy may impair diagnostic accuracy. However, a newly detected hypermetabolism weeks after resection or treatment indicates a recurrent tumor or progression from low-grade to high-grade glioma (*121,157,158*). With a sensitivity of 75% and a specificity of 81%, ^{18}F-FDG combined to MRI can distinguish recurrent tumor from radiation necrosis (*159*). Again, ^{11}C-MET PET is more sensitive than ^{18}F-FDG PET for differentiating between recurrent tumor and radiation necrosis (Fig. 9) (*130,132*), despite limitations in tumor grading (*160*), and is especially effective in combination with MRI (*161*). Even in brain lesions that did not show increased uptake on ^{18}F-FDG PET, a sensitivity of between 89% (tumors) and 92% (gliomas) and a specificity of 100% was obtained (*162,163*).

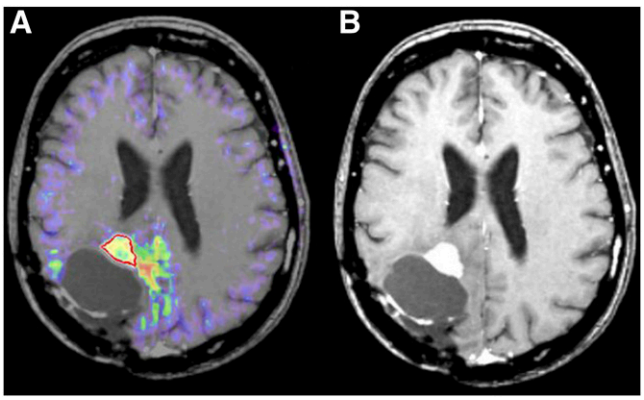

FIGURE 9. Patient with glioma after surgery and radiation. Coregistered ^{11}C-MET PET and MR images (A) demonstrate amino acid uptake medial to area of contrast enhancement (B). Biopsy showed recurrent tumor in this area.

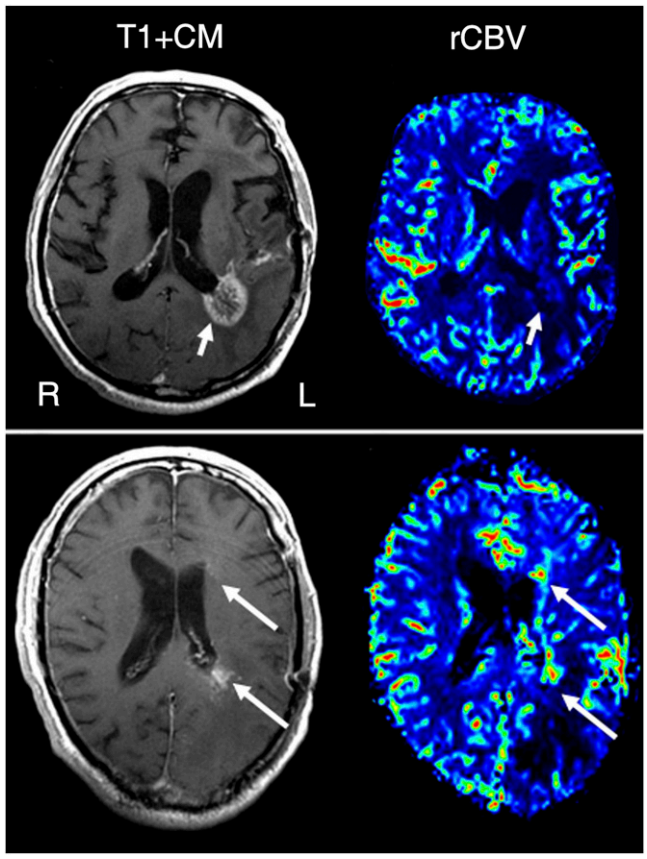

FIGURE 10. T1-weighted contrast-enhanced (T1+CM) and rCBV MR images showing radiation necrosis with low rCBV values (top row) and recurrent tumor with rCBV elevation along left ventricular wall (bottom row).

MRI

Early postsurgical imaging within 24–72 h is advised for the detection of residual contrast-enhancing tumor masses using conventional techniques. After 72 h, the amount of postsurgical granulation tissue is increasing, confounding the interpretation regarding residual tumor. Within the first 24 h after surgery, contrast enhancement can be caused by the surgical procedure itself; therefore, imaging should be avoided during this period.

It is important to characterize biologic changes in the tissue to be able to separate therapy-induced necrosis or changes from recurrence (Fig. 10). Signs of newly increased cell membrane turnover, new disruptions of BBB, new angiogenesis, and increased perfusion can indicate tumor recurrence. Histopathologically, radiation necrosis is characterized by endothelial damage and fibrinoid necrosis, whereas recurrent tumor contains increased microvasculature, as do primary high-grade brain tumors. One study found rCBV measure-

ments to be equivalent to ^{11}C-MET PET in the follow-up of patients with high-grade gliomas (*164*). In a recent 12-patient study assessing progression of gliomas after resection and radiochemotherapy, MRS was more accurate in low-grade gliomas and ^{18}F-FDG PET was more accurate in high-grade gliomas (*165*).

A comprehensive review of multimodal imaging for the assessment of treatment response in gliomas was published recently (*166*).

New, evolving MRI techniques such as imaging of endogenous proteins and peptides might further help in the differentiation of glioma and radiation necrosis. In an animal model, detection of amide protons by a new technique called amide proton transfer MRI was shown to provide a biomarker for tissue characterization in this situation (*167*). Amide proton transfer MRI is based on a contrast mechanism called chemical exchange–dependent saturation transfer (*168*) and can easily be incorporated into routine clinical examination without the use of exogenous contrast material (*169*).

THE FUTURE: HYBRID PET/MRI SYSTEMS

The results of coregistration of PET and MRI data prove the added value of multimodality imaging, but this value is affected by the necessity of positioning the patient in different scanners, often in different physiological conditions and at different times. These problems are solved by hybrid PET/MRI systems that combine the excellent soft-tissue contrast at high resolution of MRI and its additional imaging options such as spectroscopy, functional MRI, diffusion- and perfusion-weighted imaging with the molecular, biochemical, and functional information obtained by PET. In contrast to PET/CT, in which the modalities are used sequentially and the subsequent results fused, data acquisition in a hybrid PET/MRI system takes place simultaneously, since the specially constructed PET detectors (*170*) are placed within the MRI scanner. The PET detectors must be invisible to the MRI scanner and must not interfere with the field gradients or MR radiofrequency pulses. The MRI scanner must be adapted to accommodate the PET detectors, with radiofrequency coils built for minimal interference with the PET electronics (*171*). Additionally, completely new strategies for PET attenuation correction based on MRI information had to be developed (*172*). After the feasibility of simultaneous PET/MRI was demonstrated (*2*), a series of dedicated brain PET/MRI scanners was installed and some of the many promising applications (*173*) were tested. The high resolving power of the hybrid system was reported in the first clinical studies (*174*), which demonstrated simultaneous structural, functional, and molecular imaging in patients with brain tumors. The combination of PET and MRI into a single system allows for better MRI-based motion correction of PET data. The results can be used to define biopsy targets and to better separate tumor tissue from scarring, inflammation, and necrosis. Further development is directed toward a fully integrated whole-body PET/MRI system that will use the manifold properties of simultaneous multimodal imaging (*175*) in general oncology.

SUMMARY

Conventional MRI is the preferred basis for diagnosis and follow-up of brain tumors. Dedicated PET and elaborate MRI procedures, which can be used to analyze physiologic and metabolic changes in healthy and pathologic tissue, are valuable complementary tools enabling better grading of brain tumors, monitoring of treatment effects, and detection of recurrences. Fully integrated whole-body PET/MRI systems will soon be available to combine the advantages of both techniques in a single step.

ACKNOWLEDGMENT

This work was supported in part by a grant from the WDH Foundation, Cologne.

REFERENCES

1. Beyer T, Townsend DW, Brun T, et al. A combined PET/CT scanner for clinical oncology. *J Nucl Med.* 2000;41:1369–1379.
2. Schlemmer HP, Pichler BJ, Schmand M, et al. Simultaneous MR/PET imaging of the human brain: feasibility study. *Radiology.* 2008;248:1028–1035.
3. Kleihues P, Cavenee WK. *Tumours of the Nervous System.* Lyon, France: International Agency for Research on Cancer; 1997.
4. Louis DN, Ohgaki H, Wiestler OD, et al. The 2007 WHO classification of tumours of the central nervous system. *Acta Neuropathol.* 2007;114:97–109.
5. Paulus W, Peiffer J. Intratumoral histologic heterogeneity of gliomas: a quantitative study. *Cancer.* 1989;64:442–447.
6. Ginsberg LE, Fuller GN, Hashmi M, Leeds NE, Schomer DF. The significance of lack of MR contrast enhancement of supratentorial brain tumors in adults: histopathological evaluation of a series. *Surg Neurol.* 1998;49:436–440.
7. Scott JN, Brasher PM, Sevick RJ, Rewcastle NB, Forsyth PA. How often are nonenhancing supratentorial gliomas malignant? A population study. *Neurology.* 2002;59:947–949.
8. Tyler JL, Diksic M, Villemure JG, et al. Metabolic and hemodynamic evaluation of gliomas using positron emission tomography. *J Nucl Med.* 1987;28:1123–1133.
9. Krohn KA, Mankoff DA, Muzi M, Link JM, Spence AM. True tracers: comparing FDG with glucose and FLT with thymidine. *Nucl Med Biol.* 2005;32:663–671.
10. Patronas NJ, Di Chiro G, Brooks RA, et al. Work in progress: [^{18}F] fluorodeoxyglucose and positron emission tomography in the evaluation of radiation necrosis of the brain. *Radiology.* 1982;144:885–889.
11. Warburg O. On the origin of cancer cells. *Science.* 1956;123:309–314.
12. Delbeke D, Meyerowitz C, Lapidus RL, et al. Optimal cutoff levels of F-18 fluorodeoxyglucose uptake in the differentiation of low-grade from high-grade brain tumors with PET. *Radiology.* 1995;195:47–52.
13. Spence AM, Muzi M, Mankoff DA, et al. ^{18}F-FDG PET of gliomas at delayed intervals: improved distinction between tumor and normal gray matter. *J Nucl Med.* 2004;45:1653–1659.
14. Di Chiro G, DeLaPaz RL, Brooks RA, et al. Glucose utilization of cerebral gliomas measured by (^{18}F) fluorodeoxyglucose and positron emission tomography. *Neurology.* 1982;32:1323–1329.
15. Alavi JB, Alavi A, Chawluk J, et al. Positron emission tomography in patients with glioma: a predictor of prognosis. *Cancer.* 1988;62:1074–1078.
16. Herholz K, Pietrzyk U, Voges J, et al. Correlation of glucose consumption and tumor cell density in astrocytomas: a stereotactic PET study. *J Neurosurg.* 1993; 79:853–858.
17. Patronas NJ, Dichiro G, Kufta C, et al. Prediction of survival in glioma patients by means of positron emission tomography. *J Neurosurg.* 1985;62:816–822.
18. Barker FG II, Chang SM, Valk PE, Pounds TR, Prados MD. 18-fluorodeoxyglucose uptake and survival of patients with suspected recurrent malignant glioma. *Cancer.* 1997;79:115–126.

19. DeLaPaz RL, Patronas NJ, Brooks RA, et al. Positron emission tomography study of suppression of gray matter glucose utilization by brain tumors. *Am J Neuroradiol.* 1983;4:826–829.
20. Hölzer T, Herholz K, Jeske J, Heiss WD. FDG-PET as a prognostic indicator in radiochemotherapy of glioblastoma. *J Comput Assist Tomogr.* 1993;17:681–687.
21. Di Chiro G, Hatazawa J, Katz DA, Rizzoli HV, De Michele DJ. Glucose utilization by intracranial meningiomas as an index of tumor aggressivity and probability of recurrence: a PET study. *Radiology.* 1987;164:521–526.
22. Herholz K, Herscovitch P, Heiss WD. *NeuroPET: Positron Emission Tomography in Neuroscience and Clinical Neurology.* Berlin, Germany: Springer; 2004.
23. Ullrich RT, Kracht LW, Jacobs AH. Neuroimaging in patients with gliomas. *Semin Neurol.* 2008;28:484–494.
24. Miyagawa T, Oku T, Uehara H, et al. "Facilitated" amino acid transport is upregulated in brain tumors. *J Cereb Blood Flow Metab.* 1998;18:500–509.
25. Bading JR, Kan-Mitchell J, Conti PS. System A amino acid transport in cultured human tumor cells: implications for tumor imaging with PET. *Nucl Med Biol.* 1996;23:779–786.
26. Herholz K, Holzer T, Bauer B, et al. ^{11}C-methionine PET for differential diagnosis of low-grade gliomas. *Neurology.* 1998;50:1316–1322.
27. Kaschten B, Stevenaert A, Sadzot B, et al. Preoperative evaluation of 54 gliomas by PET with fluorine-18-fluorodeoxyglucose and/or carbon-11-methionine. *J Nucl Med.* 1998;39:778–785.
28. Sasaki M, Kuwabara Y, Yoshida T, et al. Carbon-11-methionine PET in focal cortical dysplasia: a comparison with fluorine-18-FDG PET and technetium-99m-ECD SPECT. *J Nucl Med.* 1998;39:974–977.
29. Bustany P, Chatel M, Derlon JM, et al. Brain tumor protein synthesis and histological grades: a study by positron emission tomography (PET) with C11-L-methionine. *J Neurooncol.* 1986;3:397–404.
30. Ogawa T, Inugami A, Hatazawa J, et al. Clinical positron emission tomography for brain tumors: comparison of fludeoxyglucose F 18 and L-methyl-^{11}C-methionine. *AJNR.* 1996;17:345–353.
31. Chang CC, Kuwana N, Ito S, Yokoyama T, Kanno H, Yamamoto I. Cerebral haemodynamics in patients with hydrocephalus after subarachnoid haemorrhage due to ruptured aneurysm. *Eur J Nucl Med Mol Imaging.* 2003;30:123–126.
32. Kracht LW, Friese M, Herholz K, et al. Methyl-(^{11}C)-L-methionine uptake as measured by positron emission tomography correlates to microvessel density in patients with glioma. *Eur J Nucl Med Mol Imaging.* 2003;30:868–873.
33. Ericson K, Lilja A, Bergström M, et al. Positron emission tomography with ([^{11}C]methyl)-L-methionine, [^{11}C]D-glucose, and [^{68}Ga]EDTA in supratentorial tumors. *J Comput Assist Tomogr.* 1985;9:683–689.
34. De Witte O, Goldberg I, Wikler D, et al. Positron emission tomography with injection of methionine as a prognostic factor in glioma. *J Neurosurg.* 2001;95:746–750.
35. Ribom D, Eriksson A, Hartman M, et al. Positron emission tomography ^{11}C-methionine and survival in patients with low-grade gliomas. *Cancer.* 2001;92:1541–1549.
36. Galldiks N, Kracht LW, Berthold F, et al. [^{11}C]-L-methionine positron emission tomography in the management of children and young adults with brain tumors. *J Neurooncol.* 2010;96:231–239.
37. Stadlbauer A, Prante O, Nimsky C, et al. Metabolic imaging of cerebral gliomas: spatial correlation of changes in O-(2-^{18}F-fluoroethyl)-L-tyrosine PET and proton magnetic resonance spectroscopic imaging. *J Nucl Med.* 2008;49:721–729.
38. Derlon JM, Petit-Taboue MC, Chapon F, et al. The in vivo metabolic pattern of low-grade brain gliomas: a positron emission tomographic study using ^{18}F-fluorodeoxyglucose and ^{11}C-L-methylmethionine. *Neurosurgery.* 1997;40:276–287.
39. Kato T, Shinoda J, Oka N, et al. Analysis of ^{11}C-methionine uptake in low-grade gliomas and correlation with proliferative activity. *AJNR.* 2008;29:1867–1871.
40. Weber WA, Wester HJ, Grosu AL, et al. O-(2-[^{18}F]fluoroethyl)-L-tyrosine and L-[methyl-^{11}C]methionine uptake in brain tumours: initial results of a comparative study. *Eur J Nucl Med.* 2000;27:542–549.
41. Becherer A, Karanikas G, Szabo M, et al. Brain tumour imaging with PET: a comparison between [^{18}F]fluorodopa and [^{11}C]methionine. *Eur J Nucl Med Mol Imaging.* 2003;30:1561–1567.
42. Chen W, Silverman DH, Delaloye S, et al. ^{18}F-FDOPA PET imaging of brain tumors: comparison study with ^{18}F-FDG PET and evaluation of diagnostic accuracy. *J Nucl Med.* 2006;47:904–911.
43. Fueger BJ, Czernin J, Cloughesy T, et al. Correlation of 6-^{18}F-fluoro-L-dopa PET uptake with proliferation and tumor grade in newly diagnosed and recurrent gliomas. *J Nucl Med.* 2010;51:1532–1538.
44. Shields AF, Grierson JR, Dohmen BM, et al. Imaging proliferation in vivo with [^{18}F] FLT and positron emission tomography. *Nat Med.* 1998;4:1334–1336.
45. Rasey JS, Grierson JR, Wiens LW, Kolb PD, Schwartz JL. Validation of FLT uptake as a measure of thymidine kinase-1 activity in A549 carcinoma cells. *J Nucl Med.* 2002;43:1210–1217.
46. Ullrich R, Backes H, Li H, et al. Glioma proliferation as assessed by 3′-fluoro-3′-deoxy-L-thymidine positron emission tomography in patients with newly diagnosed high-grade glioma. *Clin Cancer Res.* 2008;14:2049–2055.
47. Chen W, Cloughesy T, Kamdar N, et al. Imaging proliferation in brain tumors with ^{18}F-FLT PET: comparison with ^{18}F-FDG. *J Nucl Med.* 2005;46:945–952.
48. Jacobs AH, Thomas A, Kracht LW, et al. ^{18}F-fluoro-L-thymidine and ^{11}C-methylmethionine as markers of increased transport and proliferation in brain tumors. *J Nucl Med.* 2005;46:1948–1958.
49. Hatakeyama T, Kawai N, Nishiyama Y, et al. ^{11}C-methionine (MET) and ^{18}F-fluorothymidine (FLT) PET in patients with newly diagnosed glioma. *Eur J Nucl Med Mol Imaging.* 2008;35:2009–2017.
50. Valk PE, Mathis CA, Prados MD, Gilbert JC, Budinger TF. Hypoxia in human gliomas: demonstration by PET with fluorine-18-fluoromisonidazole. *J Nucl Med.* 1992;33:2133–2137.
51. Bruehlmeier M, Roelcke U, Schubiger PA, Ametamey SM. Assessment of hypoxia and perfusion in human brain tumors using PET with ^{18}F-fluoromisonidazole and ^{15}O-H_2O. *J Nucl Med.* 2004;45:1851–1859.
52. Cher LM, Murone C, Lawrentschuk N, et al. Correlation of hypoxic cell fraction and angiogenesis with glucose metabolic rate in gliomas using ^{18}F-fluoromisonidazole, ^{18}F-FDG PET, and immunohistochemical studies. *J Nucl Med.* 2006;47:410–418.
53. Szeto MD, Chakraborty G, Hadley J, et al. Quantitative metrics of net proliferation and invasion link biological aggressiveness assessed by MRI with hypoxia assessed by FMISO-PET in newly diagnosed glioblastomas. *Cancer Res.* 2009;69:4502–4509.
54. Spence AM, Muzi M, Swanson KR, et al. Regional hypoxia in glioblastoma multiforme quantified with [^{18}F]fluoromisonidazole positron emission tomography before radiotherapy: correlation with time to progression and survival. *Clin Cancer Res.* 2008;14:2623–2630.
55. Henze M, Schuhmacher J, Hipp P, et al. PET imaging of somatostatin receptors using [^{68}GA]DOTA-D-Phe1-Tyr3-octreotide: first results in patients with meningiomas. *J Nucl Med.* 2001;42:1053–1056.
56. Nyuyki F, Plotkin M, Graf R, et al. Potential impact of ^{68}Ga-DOTATOC PET/CT on stereotactic radiotherapy planning of meningiomas. *Eur J Nucl Med Mol Imaging.* 2010;37:310–318.
57. Milker-Zabel S, Zabel-du Bois A, Henze M, et al. Improved target volume definition for fractionated stereotactic radiotherapy in patients with intracranial meningiomas by correlation of CT, MRI, and [^{68}Ga]-DOTATOC-PET. *Int J Radiat Oncol Biol Phys.* 2006;65:222–227.
58. Thorwarth D, Henke G, Müller AC, et al. Simultaneous ^{68}Ga-DOTATOC-PET/MRI for IMRT treatment planning for meningioma: first experience. *Int J Radiat Oncol Biol Phys.* February 5, 2011 [Epub ahead of print].
59. Herminghaus S, Dierks T, Pilatus U, et al. Determination of histopathological tumor grade in neuroepithelial brain tumors by using spectral pattern analysis of in vivo spectroscopic data. *J Neurosurg.* 2003;98:74–81.
60. Usenius JP, Tuohimetsa S, Vainio P, Ala-Korpela M, Hiltunen Y, Kauppinen RA. Automated classification of human brain tumours by neural network analysis using in vivo ^{1}H magnetic resonance spectroscopic metabolite phenotypes. *Neuroreport.* 1996;7:1597–1600.
61. Li X, Lu Y, Pirzkall A, McKnight T, Nelson SJ. Analysis of the spatial characteristics of metabolic abnormalities in newly diagnosed glioma patients. *J Magn Reson Imaging.* 2002;16:229–237.
62. Herminghaus S, Pilatus U, Moller-Hartmann W, et al. Increased choline levels coincide with enhanced proliferative activity of human neuroepithelial brain tumors. *NMR Biomed.* 2002;15:385–392.
63. Shimizu H, Kumabe T, Shirane R, Yoshimoto T. Correlation between choline level measured by proton MR spectroscopy and Ki-67 labeling index in gliomas. *AJNR.* 2000;21:659–665.
64. Porto L, Kieslich M, Franz K, et al. Spectroscopy of untreated pilocytic astrocytomas: do children and adults share some metabolic features in addition to their morphologic similarities? *Childs Nerv Syst.* 2010;26:801–806.
65. Xu M, See SJ, Ng WH, et al. Comparison of magnetic resonance spectroscopy and perfusion-weighted imaging in presurgical grading of oligodendroglial tumors. *Neurosurgery.* 2005;56:919–926.
66. Hattingen E, Delic O, Franz K, et al. ^{1}H MRSI and progression-free survival in patients with WHO grades II and III gliomas. *Neurol Res.* 2010;32:593–602.
67. Hattingen E, Raab P, Franz K, et al. Prognostic value of choline and creatine in WHO grade II gliomas. *Neuroradiology.* 2008;50:759–767.
68. Burtscher IM, Skagerberg G, Geijer B, et al. Spectroscopy and preoperative diagnostic accuracy: an evaluation of intracranial mass lesions characterized by stereotactic biopsy findings. *AJNR* 2000;21:84–93.
69. Hermann EJ, Hattingen E, Krauss JK, et al. Stereotactic biopsy in gliomas guided by 3-tesla ^{1}H-chemical-shift imaging of choline. *Stereotact Funct Neurosurg.* 2008;86:300–307.

70. Hattingen E, Raab P, Franz K, Zanella FE, Lanfermann H, Pilatus U. Myo-inositol: a marker of reactive astrogliosis in glial tumors? *NMR Biomed.* 2008; 21:233–241.
71. Nelson SJ, Graves E, Pirzkall A, et al. In vivo molecular imaging for planning radiation therapy of gliomas: an application of ^{1}H MRSI. *J Magn Reson Imaging.* 2002;16:464–476.
72. Chawla S, Zhang Y, Wang S, et al. Proton magnetic resonance spectroscopy in differentiating glioblastomas from primary cerebral lymphomas and brain metastases. *J Comput Assist Tomogr.* 2010;34:836–841.
73. Day SE, Kettunen MI, Cherukuri MK, et al. Detecting response of rat C6 glioma tumors to radiotherapy using hyperpolarized [1-^{13}C]pyruvate and ^{13}C magnetic resonance spectroscopic imaging. *Magn Reson Med.* 2011;65:557–563.
74. Witney TH, Kettunen MI, Day SE, et al. A comparison between radiolabeled fluorodeoxyglucose uptake and hyperpolarized ^{13}C-labeled pyruvate utilization as methods for detecting tumor response to treatment. *Neoplasia* 2009;11: 574–582.
75. Le Bihan D. Molecular diffusion, tissue microdynamics and microstructure. *NMR Biomed.* 1995;8:375–386.
76. Arvinda HR, Kesavadas C, Sarma PS, et al. Glioma grading: sensitivity, specificity, positive and negative predictive values of diffusion and perfusion imaging. *J Neurooncol.* 2009;94:87–96.
77. Koral K, Gargan L, Bowers DC, et al. Imaging characteristics of atypical teratoid-rhabdoid tumor in children compared with medulloblastoma. *AJR.* 2008;190:809–814.
78. Rumboldt Z, Camacho DL, Lake D, Welsh CT, Castillo M. Apparent diffusion coefficients for differentiation of cerebellar tumors in children. *AJNR.* 2006; 27:1362–1369.
79. Kocaoglu M, Ors F, Bulakbasi N, Onguru O, Ulutin C, Secer HI. Central neurocytoma: proton MR spectroscopy and diffusion weighted MR imaging findings. *Magn Reson Imaging.* 2009;27:434–440.
80. Jensen JH, Helpern JA. MRI quantification of non-Gaussian water diffusion by kurtosis analysis. *NMR Biomed.* 2010;23:698–710.
81. Raab P, Hattingen E, Franz K, Zanella FE, Lanfermann H. Cerebral gliomas: diffusional kurtosis imaging analysis of microstructural differences. *Radiology.* 2010;254:876–881.
82. Cha S, Knopp EA, Johnson G, Wetzel SG, Litt AW, Zagzag D. Intracranial mass lesions: dynamic contrast-enhanced susceptibility-weighted echo-planar perfusion MR imaging. *Radiology.* 2002;223:11–29.
83. Boxerman JL, Schmainda KM, Weisskoff RM. Relative cerebral blood volume maps corrected for contrast agent extravasation significantly correlate with glioma tumor grade, whereas uncorrected maps do not. *AJNR.* 2006;27:859–867.
84. Hu LS, Baxter LC, Pinnaduwage DS, et al. Optimized preload leakage-correction methods to improve the diagnostic accuracy of dynamic susceptibility-weighted contrast-enhanced perfusion MR imaging in posttreatment gliomas. *AJNR.* 2010;31:40–48.
85. Tofts PS, Brix G, Buckley DL, et al. Estimating kinetic parameters from dynamic contrast-enhanced T(1)-weighted MRI of a diffusable tracer: standardized quantities and symbols. *J Magn Reson Imaging.* 1999;10:223–232.
86. Cao Y, Shen Z, Chenevert TL, Ewing JR. Estimate of vascular permeability and cerebral blood volume using Gd-DTPA contrast enhancement and dynamic T2*-weighted MRI. *J Magn Reson Imaging.* 2006;24:288–296.
87. Law M, Yang S, Wang H, et al. Glioma grading: sensitivity, specificity, and predictive values of perfusion MR imaging and proton MR spectroscopic imaging compared with conventional MR imaging. *AJNR.* 2003;24:1989–1998.
88. Provenzale JM, York G, Moya MG, et al. Correlation of relative permeability and relative cerebral blood volume in high-grade cerebral neoplasms. *AJR.* 2006;187:1036–1042.
89. Roberts C, Issa B, Stone A, Jackson A, Waterton JC, Parker GJ. Comparative study into the robustness of compartmental modeling and model-free analysis in DCE-MRI studies. *J Magn Reson Imaging.* 2006;23:554–563.
90. Spampinato MV, Smith JK, Kwock L, et al. Cerebral blood volume measurements and proton MR spectroscopy in grading of oligodendroglial tumors. *AJR.* 2007;188:204–212.
91. Law M, Yang S, Babb JS, et al. Comparison of cerebral blood volume and vascular permeability from dynamic susceptibility contrast-enhanced perfusion MR imaging with glioma grade. *AJNR.* 2004;25:746–755.
92. Patankar TF, Haroon HA, Mills SJ, et al. Is volume transfer coefficient (K(trans)) related to histologic grade in human gliomas? *AJNR.* 2005;26:2455–2465.
93. Saitta L, Heese O, Förster AF, et al. Signal intensity in T2′ magnetic resonance imaging is related to brain glioma grade. *Eur Radiol.* 2011;21:1068–1076.
94. Siemonsen S, Fitting T, Thomalla G, et al. T2′ imaging predicts infarct growth beyond the acute diffusion-weighted imaging lesion in acute stroke. *Radiology.* 2008;248:979–986.
95. Levivier M, Goldman S, Pirotte B, et al. Diagnostic yield of stereotactic brain biopsy guided by positron emission tomography with [^{18}F]fluorodeoxyglucose. *J Neurosurg.* 1995;82:445–452.
96. Widhalm G, Krssak M, Minchev G, et al. Value of ^{1}H-magnetic resonance spectroscopy chemical shift imaging for detection of anaplastic foci in diffusely infiltrating gliomas with non-significant contrast-enhancement. *J Neurol Neurosurg Psychiatry.* 2011;82:512–520.
97. Lupo JM, Cha S, Chang SM, Nelson SJ. Dynamic susceptibility-weighted perfusion imaging of high-grade gliomas: characterization of spatial heterogeneity. *AJNR.* 2005;26:1446–1454.
98. Goldman S, Levivier M, Pirotte B, et al. Regional methionine and glucose uptake in high-grade gliomas: a comparative study on PET-guided stereotaxic biopsy. *J Nucl Med.* 1997;38:1459–1462.
99. Pirotte B, Goldman S, Massager N, et al. Comparison of ^{18}F-FDG and ^{11}C-methionine for PET-guided stereotactic brain biopsy of gliomas. *J Nucl Med.* 2004;45:1293–1298.
100. Mineura K, Sasajima T, Kowada M, Uesaka Y, Shishido F. Innovative approach in the diagnosis of gliomatosis cerebri using carbon-11-L-methionine positron emission tomography. *J Nucl Med.* 1991;32:726–728.
101. Pauleit D, Floeth F, Hamacher K, et al. O-(2-[^{18}F]fluoroethyl)-L-tyrosine PET combined with MRI improves the diagnostic assessment of cerebral gliomas. *Brain.* 2005;128:678–687.
102. Floeth FW, Pauleit D, Wittsack HJ, et al. Multimodal metabolic imaging of cerebral gliomas: positron emission tomography with [^{18}F]fluoroethyl-L-tyrosine and magnetic resonance spectroscopy. *J Neurosurg.* 2005;102:318–327.
103. Kracht LW, Miletic H, Busch S, et al. Delineation of brain tumor extent with [^{11}C]L-methionine positron emission tomography: local comparison with stereotactic histopathology. *Clin Cancer Res.* 2004;10:7163–7170.
104. Roelcke U, Blasberg RG, von Ammon K, et al. Dexamethasone treatment and plasma glucose levels: relevance for fluorine-18-fluorodeoxyglucose uptake measurements in gliomas. *J Nucl Med.* 1998;39:879–884.
105. Pietrzyk U, Herholz K, Heiss WD. Three-dimensional alignment of functional and morphological tomograms. *J Comput Assist Tomogr.* 1990;14:51–59.
106. Heiss WD, Thiel A. A proposed regional hierarchy in recovery of post-stroke aphasia. *Brain Lang.* 2006;98:118–123.
107. Wunderlich G, Knorr U, Herzog H, Kiwit JC, Freund HJ, Seitz RJ. Precentral glioma location determines the displacement of cortical hand representation. *Neurosurgery* 1998;42:18–26.
108. Thiel A, Herholz K, von Stockhausen HM, et al. Localization of language-related cortex with ^{15}O-labeled water PET in patients with gliomas. *Neuroimage.* 1998;7:284–295.
109. Thiel A, Herholz K, Koyuncu A, et al. Plasticity of language networks in patients with brain tumors: a PET activation study. *Ann Neurol.* 2001;50:620–629.
110. Thiel A, Habedank B, Winhuisen L, et al. Essential language function of the right hemisphere in brain tumor patients. *Ann Neurol.* 2005;57:128–131.
111. Thiel A, Habedank B, Herholz K, et al. From the left to the right: how the brain compensates progressive loss of language function. *Brain Lang.* 2006;98:57–65.
112. Binder JR, Swanson SJ, Hammeke TA, et al. Determination of language dominance using functional MRI: a comparison with the Wada test. *Neurology.* 1996;46:978–984.
113. Byrnes TJ, Barrick TR, Bell BA, Clark CA. Diffusion tensor imaging discriminates between glioblastoma and cerebral metastases in vivo. *NMR Biomed.* 2011;24:54–60.
114. Law M, Oh S, Babb JS, et al. Low-grade gliomas: dynamic susceptibility-weighted contrast-enhanced perfusion MR imaging—prediction of patient clinical response. *Radiology.* 2006;238:658–667.
115. Law M, Young RJ, Babb JS, et al. Gliomas: predicting time to progression or survival with cerebral blood volume measurements at dynamic susceptibility-weighted contrast-enhanced perfusion MR imaging. *Radiology.* 2008;247:490–498.
116. Danchaivijitr N, Waldman AD, Tozer DJ, et al. Low-grade gliomas: do changes in rCBV measurements at longitudinal perfusion-weighted MR imaging predict malignant transformation? *Radiology.* 2008;247:170–178.
117. Tzika AA, Astrakas LG, Zarifi MK, et al. Spectroscopic and perfusion magnetic resonance imaging predictors of progression in pediatric brain tumors. *Cancer.* 2004;100:1246–1256.
118. Pope WB, Kim HJ, Huo J, et al. Recurrent glioblastoma multiforme: ADC histogram analysis predicts response to bevacizumab treatment. *Radiology.* 2009;252:182–189.
119. Würker M, Herholz K, Voges J, et al. Glucose consumption and methionine uptake in low-grade gliomas after iodine-125 brachytherapy. *Eur J Nucl Med.* 1996;23:583–586.
120. Brock CS, Young H, O'Reilly SM, et al. Early evaluation of tumour metabolic response using [^{18}F]fluorodeoxyglucose and positron emission tomography: a pilot study following the phase II chemotherapy schedule for temozolomide in recurrent high-grade gliomas. *Br J Cancer.* 2000;82:608–615.

121. Glantz MJ, Hoffman JM, Coleman RE, et al. Identification of early recurrence of primary central-nervous-system tumors by [^{18}F] fluorodeoxyglucose positron emission tomography. *Ann Neurol.* 1991;29:347–355.
122. Ricci PE, Karis JP, Heiserman JE, Fram EK, Bice AN, Drayer BP. Differentiating recurrent tumor from radiation necrosis: time for re-evaluation of positron emission tomography. *AJNR.* 1998;19:407–413.
123. Tanaka Y, Nariai T, Momose T, et al. Glioma surgery using a multimodal navigation system with integrated metabolic images. *J Neurosurg.* 2009;110: 163–172.
124. Grosu AL, Weber WA, Riedel E, et al. L-(methyl-^{11}C) methionine positron emission tomography for target delineation in resected high-grade gliomas before radiotherapy. *Int J Radiat Oncol Biol Phys.* 2005;63:64–74.
125. Weber DC, Zilli T, Buchegger F, et al. [^{18}F]fluoroethyltyrosine-positron emission tomography-guided radiotherapy for high-grade glioma. *Radiat Oncol.* 2008;3:44.
126. Vees H, Senthamizhchelvan S, Miralbell R, Weber DC, Ratib O, Zaidi H. Assessment of various strategies for ^{18}F-FET PET-guided delineation of target volumes in high-grade glioma patients. *Eur J Nucl Med Mol Imaging.* 2009; 36:182–193.
127. Nariai T, Tanaka Y, Wakimoto H, et al. Usefulness of L-[methyl-^{11}C] methionine-positron emission tomography as a biological monitoring tool in the treatment of glioma. *J Neurosurg.* 2005;103:498–507.
128. Pirotte BJ, Levivier M, Goldman S, et al. Positron emission tomography-guided volumetric resection of supratentorial high-grade gliomas: a survival analysis in 66 consecutive patients. *Neurosurgery.* 2009;64:471–481.
129. Thiel A, Pietrzyk U, Sturm V, Herholz K. Hövels M, Schröder R. Enhanced accuracy in differential diagnosis of radiation necrosis by positron emission tomography-magnetic resonance imaging coregistration: technical case report. *Neurosurgery.* 2000;46:232–234.
130. Tsuyuguchi N, Takami T, Sunada I, et al. Methionine positron emission tomography for differentiation of recurrent brain tumor and radiation necrosis after stereotactic radiosurgery: in malignant glioma. *Ann Nucl Med.* 2004;18:291–296.
131. Terakawa Y, Tsuyuguchi N, Iwai Y, et al. Diagnostic accuracy of ^{11}C-methionine PET for differentiation of recurrent brain tumors from radiation necrosis after radiotherapy. *J Nucl Med.* 2008;49:694–699.
132. Van Laere K, Ceyssens S, Van Calenbergh F, et al. Direct comparison of ^{18}F-FDG and ^{11}C-methionine PET in suspected recurrence of glioma: sensitivity, inter-observer variability and prognostic value. *Eur J Nucl Med Mol Imaging.* 2005;32:39–51.
133. Ullrich RT, Kracht L, Brunn A, et al. Methyl-L-^{11}C-methionine PET as a diagnostic marker for malignant progression in patients with glioma. *J Nucl Med.* 2009;50:1962–1968.
134. Galldiks N, Ullrich R, Schroeter M, Fink GR, Jacobs AH, Kracht LW. Volumetry of [^{11}C]-methionine PET uptake and MRI contrast enhancement in patients with recurrent glioblastoma multiforme. *Eur J Nucl Med Mol Imaging.* 2010;37:84–92.
135. Yamane T, Sakamoto S, Senda M. Clinical impact of ^{11}C-methionine PET on expected management of patients with brain neoplasm. *Eur J Nucl Med Mol Imaging.* 2010;37:685–690.
136. Galldiks N, Kracht L, Burghaus L, et al. Use of ^{11}C-methionine PET to monitor the effects of temozolomide chemotherapy in malignant gliomas. *Eur J Nucl Med Mol Imaging.* 2006;33:516–524.
137. Wyss M, Hofer S, Bruehlmeier M, et al. Early metabolic responses in temozolomide treated low-grade glioma patients. *J Neurooncol.* 2009;95:87–93.
138. Galldiks N, Kracht LW, Burghaus L, et al. Patient-tailored, imaging-guided, long-term temozolomide chemotherapy in patients with glioblastoma. *Mol Imaging.* 2010;9:40–46.
139. Rachinger W, Goetz C, Popperl G, et al. Positron emission tomography with O-(2-[^{18}F]fluoroethyl)-l-tyrosine versus magnetic resonance imaging in the diagnosis of recurrent gliomas. *Neurosurgery.* 2005;57:505–511.
140. Mehrkens JH, Popperl G, Rachinger W, et al. The positive predictive value of O-(2-[^{18}F]fluoroethyl)-L-tyrosine (FET) PET in the diagnosis of a glioma recurrence after multimodal treatment. *J Neurooncol.* 2008;88:27–35.
141. Chen W, Delaloye S, Silverman DH, et al. Predicting treatment response of malignant gliomas to bevacizumab and irinotecan by imaging proliferation with [^{18}F] fluorothymidine positron emission tomography: a pilot study. *J Clin Oncol.* 2007;25:4714–4721.
142. Schnell O, Krebs B, Carlsen J, et al. Imaging of integrin alpha$_v$beta$_3$ expression in patients with malignant glioma by [^{18}F] galacto-RGD positron emission tomography. *Neuro Oncol.* 2009;11:861–870.
143. Jacobs A, Voges J, Reszka R, et al. Positron-emission tomography of vector-mediated gene expression in gene therapy for gliomas. *Lancet.* 2001;358:727–729.
144. van den Bent MJ, Vogelbaum MA, Wen PY, Macdonald DR, Chang SM. End point assessment in gliomas: novel treatments limit usefulness of classical Macdonald's criteria. *J Clin Oncol.* 2009;27:2905–2908.
145. Taal W, Brandsma D, de Bruin HG, et al. Incidence of early pseudo-progression in a cohort of malignant glioma patients treated with chemoirradiation with temozolomide. *Cancer.* 2008;113:405–410.
146. Hamstra DA, Chenevert TL, Moffat BA, et al. Evaluation of the functional diffusion map as an early biomarker of time-to-progression and overall survival in high-grade glioma. *Proc Natl Acad Sci USA.* 2005;102:16759–16764.
147. Hamstra DA, Galban CJ, Meyer CR, et al. Functional diffusion map as an early imaging biomarker for high-grade glioma: correlation with conventional radiologic response and overall survival. *J Clin Oncol.* 2008;26:3387–3394.
148. Moffat BA, Chenevert TL, Lawrence TS, et al. Functional diffusion map: a noninvasive MRI biomarker for early stratification of clinical brain tumor response. *Proc Natl Acad Sci USA.* 2005;102:5524–5529.
149. Chenevert TL, Stegman LD, Taylor JM, et al. Diffusion magnetic resonance imaging: an early surrogate marker of therapeutic efficacy in brain tumors. *J Natl Cancer Inst.* 2000;92:2029–2036.
150. Cao Y, Tsien CI, Nagesh V, et al. Survival prediction in high-grade gliomas by MRI perfusion before and during early stage of RT. *Int J Radiat Oncol Biol Phys.* 2006;64:876–885.
151. Galban CJ, Chenevert TL, Meyer CR, et al. The parametric response map is an imaging biomarker for early cancer treatment outcome. *Nat Med.* 2009;15:572–576.
152. Wu J, Gilbert MR, De Groot JF, Yung WA, Puduvalli VK. Diffusion restriction as a predictor of response in recurrent glioblastoma patients receiving bevacizumab [abstract]. *J Clin Oncol.* 2010;28(15 suppl):2024.
153. Rieger J, Bahr O, Muller K, Franz K, Steinbach J, Hattingen E. Bevacizumab-induced diffusion-restricted lesions in malignant glioma patients. *J Neurooncol.* 2010;99:49–56.
154. Nowosielski M, Recheis W, Goebel G, et al. ADC histograms predict response to anti-angiogenic therapy in patients with recurrent high-grade glioma. *Neuroradiology.* 2010;53:291–302.
155. Norden AD, Young GS, Setayesh K, et al. Bevacizumab for recurrent malignant gliomas: efficacy, toxicity, and patterns of recurrence. *Neurology.* 2008;70:779–787.
156. Levivier M, Becerra A, De Witte O, Brotchi J, Goldman S. Radiation necrosis or recurrence. *J Neurosurg.* 1996;84:148–149.
157. De Witte O, Levivier M, Violon P, et al. Prognostic value of positron emission tomography with [^{18}F]fluoro-2-deoxy-D-glucose in the low-grade glioma. *Neurosurgery.* 1996;39:470–476.
158. Langleben DD, Segall GM. PET in differentiation of recurrent brain tumor from radiation injury. *J Nucl Med.* 2000;41:1861–1867.
159. Chao ST, Suh JH, Raja S, Lee SY, Barnett G. The sensitivity and specificity of FDG PET in distinguishing recurrent brain tumor from radionecrosis in patients treated with stereotactic radiosurgery. *Int J Cancer.* 2001;96:191–197.
160. Ceyssens S, Van Laere K, de Groot T, Goffin J, Bormans G, Mortelmans L. [^{11}C]methionine PET, histopathology, and survival in primary brain tumors and recurrence. *AJNR.* 2006;27:1432–1437.
161. Popperl G, Gotz C, Rachinger W, Gildehaus FJ, Tonn JC, Tatsch K. Value of O-(2-[^{18}F]fluoroethyl)-L-tyrosine PET for the diagnosis of recurrent glioma. *Eur J Nucl Med Mol Imaging.* 2004;31:1464–1470.
162. Chung JK, Kim YK, Kim SK, et al. Usefulness of ^{11}C-methionine PET in the evaluation of brain lesions that are hypo- or isometabolic on ^{18}F-FDG PET. *Eur J Nucl Med Mol Imaging.* 2002;29:176–182.
163. Chen W. Clinical applications of PET in brain tumors. *J Nucl Med.* 2007;48: 1468–1481.
164. Dandois V, Rommel D, Renard L, Jamart J, Cosnard G. Substitution of ^{11}C-methionine PET by perfusion MRI during the follow-up of treated high-grade gliomas: preliminary results in clinical practice. *J Neuroradiol.* 2010;37:89–97.
165. Imani F, Boada FE, Lieberman FS, Davis DK, Deeb EL, Mountz JM. Comparison of proton magnetic resonance spectroscopy with fluorine-18 2-fluorodeoxyglucose positron emission tomography for assessment of brain tumor progression. *J Neuroimaging.* December 14, 2010 [Epub ahead of print].
166. Dhermain FG, Hau P, Lanfermann H, Jacobs AH, van den Bent MJ. Advanced MRI and PET imaging for assessment of treatment response in patients with gliomas. *Lancet Neurol.* 2010;9:906–920.
167. Zhou J, Tryggestad E, Wen Z, et al. Differentiation between glioma and radiation necrosis using molecular magnetic resonance imaging of endogenous proteins and peptides. *Nat Med.* 2011;17:130–134.
168. Ward KM, Aletras AH, Balaban RS. A new class of contrast agents for MRI based on proton chemical exchange dependent saturation transfer (CEST). *J Magn Reson.* 2000;143:79–87.
169. Zhou J, Blakeley JO, Hua J, et al. Practical data acquisition method for human brain tumor amide proton transfer (APT) imaging. *Magn Reson Med.* 2008;60:842–849.
170. Judenhofer MS, Wehrl HF, Newport DF, et al. Simultaneous PET-MRI: a new approach for functional and morphological imaging. *Nat Med.* 2008;14:459–465.

171. Pichler BJ, Kolb A, Nagele T, Schlemmer HP. PET/MRI: paving the way for the next generation of clinical multimodality imaging applications. *J Nucl Med.* 2010;51:333–336.
172. Catana C, van der Kouwe A, Benner T, et al. Toward implementing an MRI-based PET attenuation-correction method for neurologic studies on the MR-PET brain prototype. *J Nucl Med.* 2010;51:1431–1438.
173. Heiss W-D. The potential of PET/MR for brain imaging. *Eur J Nucl Med Mol Imaging.* 2009;36(suppl 1):105–112.
174. Boss A, Bisdas S, Kolb A, et al. Hybrid PET/MRI of intracranial masses: initial experiences and comparison to PET/CT. *J Nucl Med.* 2010;51:1198–1205.
175. Sauter AW, Wehrl HF, Kolb A, Judenhofer MS, Pichler BJ. Combined PET/MRI: one step further in multimodality imaging. *Trends Mol Med.* 2010;16:508–515.